Spatial Energetics of Protonated LiH: Lower-Lying Potential Energy Surfaces from Valence Bond Calculations

E. Bodo, F. A. Gianturco,* and R. Martinazzo†

Department of Chemistry, The University of Rome, Citta' Universitaria, 00185 Rome, Italy

A. Forni, A. Famulari, and M. Raimondi

Department of Physical Chemistry and Electro-chemistry, University of Milan, and CNR Center CSRSRC, via Golgi 19, 20133 Milan, Italy

Received: June 21, 2000; In Final Form: October 3, 2000

The detailed features of the interaction forces within the LiH_2^+ triatomic system are calculated using the spin-coupled valence bond (SCVB) method in terms of the three Jacobi coordinates of the $LiH(LiH^+)$ and H^+/H fragments within a broad range of relative orientations and of internuclear distances. The specific features of the systems and of their asymptotic molecular fragments are examined with the view of estimating from them the collisional probabilities for producing rovibrationally excited partners with detectable radiative behavior. The possibility of having a charge-transfer process within the two electronic states of the LiH_2^+ ion is also analyzed and discussed. The calculations suggest, albeit still qualitatively, that a direct charge-transfer reaction between $LiH + H^+$ into $LiH^+ + H$ is unlikely to take place during bimolecular collisions in a low-density medium.

1. Introduction

In modern studies of early universe chemistry it is usually accepted that chemical processes began with the appearance of the first neutral molecule H_2, soon after the production of neutral atomic hydrogen, through the radiative association of protons and electrons. Because of the absence of dust or grains in the early universe the processes that lead to the formation of the first molecules are driven by elementary reactions between atomic species.[1,2] Lithium chemistry, in fact, is thought to have been initiated by the formation of Li through the radiative recombination of the ion[3]

$$Li^+ + e^- \rightarrow Li + h\nu \qquad (1)$$

a process which is also likely to be involved in the formation of LiH^+ [4]

$$Li^+ + H \rightarrow LiH^+ + h\nu \qquad (2)$$

which could in turn produce the neutral species by an exchange reaction (further discussed below in the present paper)

$$LiH^+ + H \rightarrow LiH + H^+ \qquad (3)$$

The latter product however is competitively depleted by the processes[5]

$$LiH + H^+ \rightarrow Li^+ + H_2\ (Li + H_2^+) \qquad (4)$$

$$LiH + H \rightarrow Li + H_2 \qquad (5)$$

The above list of elementary reactions already shows that ionic and neutral partners involving hydrogen (atomic and molecular) and lithium (atomic and molecular) are of importance in establishing the kinetic details of lithium chemistry in the evolution of the early universe. It therefore follows that to set up in some realistic way an evolutionary model, it is required to estimate the particles' relative abundance in the expanding universe by taking into account the chemical reactions listed above and many others that are deemed to be relevant for the present case.[6] We have already considered[7] some aspects of it by looking into the neutral reaction (eq 5) and we are currently studying the interaction forces to yield realistic estimates for the nonreactive collisional heating of neutral LiH[8] by hydrogen.

$$LiH(\nu,j) + H \rightarrow LIH(\nu',j') + H \qquad (6)$$

To carry out similar studies for the ionic species, with their markedly stronger interaction features, we therefore need to construct in a similar way the full potential energy surface (PES), or surfaces, involving the collision between LiH and a proton. This is what we shall attempt to do here focusing, at first, not so much on the full range of Jacobi coordinates that are needed to correctly handle the scattering but rather on the orientational features and charge-localization dynamics of the short range regions of the interaction. In other words, we first intend to analyze, using a strongly correlated ab initio computational method, the orientational features of the LiH^+_2 triatomic species as a function of angles and distances, but within the range of the onset of its fragmentation processes. The following section outlines our present computational method while Sections 3 and 4 will describe, respectively, the energy and spatial features of the potential energy surfaces and their rovibrational coupling characteristics. Sections 5 and 6 will further present the charge-transfer behavior and the general conclusions from our calculations.

* Professor F. A. Gianturco, Dipartimento di Chimica, Citta' Universitaria 00185, Rome, Italy. Fax: +39-06-49913305. E-mail: fagiant@caspur.it.

† On leave from Dept. of Physical Chemistry and Electro-chemistry, University of Milan, and CNR Center.

10.1021/jp0022510 CCC: $19.00
Published on Web 12/05/2000

2. The Computational Method

The basic method that we have employed to study the ionic, strongly interacting, complex of the three atoms is that of the valence bond (VB) approach within a spin coupled (SC) formulation.[9,10] This method has been described in detail elsewhere and therefore we will only give here a brief outline of it. The spin coupled wave function for N valence electrons can be written in the form:

$$\Psi_{SC}^{(SM)} = A\,[|\phi_1\rangle\,|\phi_2\rangle\cdots|\phi_N\rangle|SM\rangle] = A[|\phi\rangle|SM\rangle] \qquad (7)$$

where $|\phi_i\rangle$ represents a singly occupied nonorthogonal orbital and $|SM\rangle$ is the total spin function, which is an eigenfunction of the $\mathbf{S}^2$ and $\mathbf{S_z}$ operators corresponding to quantum numbers S and M. The total spin function is expanded as a combination of linearly independent N-electron spin eigenstates

$$|SM\rangle = \sum_{k=1}^{f_S^N} C_{Sk}|SM, k\rangle \qquad (8)$$

where the dimension of the spin space is given by:

$$f_N^S = \frac{(2S+1)N!}{\left(\frac{1}{2}N+S+1\right)!\left(\frac{1}{2}N-S\right)!} \qquad (9)$$

and the spin coupled orbitals $|\phi_i\rangle$ are expanded, as usual, in a basis set $\{\chi\}$ of dimension m

$$\phi_i = \sum_{j=1}^{m} c_{ij}\chi_j \qquad (10)$$

An ab initio SC calculation consists of the variational optimization of all the coefficients C_{sk} and c_{ij} that appear in eqs 8 and 10. In general, this is carried out simultaneously without any constraint by minimizing the energy with respect to all the parameters with an efficient modified Newton−Raphson algorithm. The SC wave function correctly accounts for almost all nondynamic correlation and, in addition, turns out to be an excellent starting point for constructing very compact, multiconfigurational descriptions of ground and excited states according to what we call the spin coupled valence bond (SCVB) model. In fact, a set of *virtual orbitals* can be added to each *occupied* orbital, either by a conventional diagonalization of effective monoelectronic operators, or by a more recently implemented perturbative multiconfigurational approach. In this way, each electron possesses its own set of virtual orbitals, and it is possible to expand any spatial vector in the form:

$$|\Phi\rangle = |\Phi_0\rangle + \sum_i\sum_{u_i}|\Phi_i^{u_i}\rangle + \sum_{i,l}\sum_{u_i u_l}|\Phi_{il}^{u_i u_l}\rangle + \cdots \qquad (11)$$

where $|\Phi_0\rangle$ is the spin coupled configuration, $|\Phi_k^{u_k}\rangle$ is the generic singly excited configuration, and so on. Thus i and l represent indexes for the occupied orbitals involved in the virtual excitations, and u_i, u_l the corresponding involved virtual orbitals. Each sum runs independently on both indexes. In an analogous fashion, the electronic wave function can be written as

$$|\Psi^{(SM)}\rangle = A\sum_{k=1}^{f_S^N}\{c_k|\Phi_0\rangle + \sum_i\sum_{u_i}c_{i,k}^{u_i}|\Phi_i^{u_i}\rangle + \sum_{i,l}\sum_{u_i u_l}c_{il;k}^{u_i u_l}|\Phi_{il}^{u_i u_l}\rangle\}|SM,k\rangle \qquad (12)$$

where A is the antisymmetrization operator and the coefficients $\{c\}$ may be determined by solving the secular problem with the conventional VB code. Since a proper functional space is employed for each electron, the SCVB expansion is generally much shorter, for a given accuracy than the conventional MO-CI.[9] The method is also applicable to excited state problems, whenever we can optimize a SC function for the excited state of interest. Therefore, if we want to correctly describe the first excited state, which will turn out to be important in the present case, we can impose an orthogonality constraint between the excited and the ground state SC wave function and optimize the excited one in the usual way. To satisfy the above constraint independently of the spin function, we can impose in the general formula (for two arbitrary spin functions k and k')

$$\langle\Psi_{SC}|\Phi_{SC}\rangle = \sum_{P\in S_N}\epsilon_P\,\langle\psi_1\psi_2\cdots\psi_N|P^r|\,\phi_1\phi_2\cdots\phi_N\rangle\,\langle SM;k|P^\sigma|SM;k'\rangle = 0 \qquad (13)$$

that $\langle\psi_1\psi_2\cdots\psi_N|P^r|\phi_1\phi_2\cdots\phi_N\rangle = 0$ holds for all permutation operators. There are many simple ways, based on orthogonality constraints between orbitals, to achieve the above conditions: for example, in the present study we found that a particularly useful method is to keep all excited orbitals in the orthogonal complement of one orbital of the ground state which, from the variational calculation, turned out to be the highest one on the energy scale.

3. Energy and Spatial Features

3.1. The Triatomic Complex. To get detailed information on the strength and anisotropy of the interaction between a LiH molecule and H^+ and on the counterpart system formed by LiH^+ interacting with a H atom, it is expedient to analyze what we know about some of the features of the LiH_2^+ global system in the same range of relative geometries. Due to the strong interactions between component atoms, the triatomic species is known to be a stable complex with respect to all of its possible fragmentation channels:

$$LiH_2^+ \rightarrow Li^+ + H_2 \qquad (14)$$

$$\rightarrow Li + H_2^+ \qquad (15)$$

$$\rightarrow LiH^+ + H \qquad (16)$$

$$\rightarrow LiH + H^+ \qquad (17)$$

The fragmentation energy with respect to the channel in eq 14 corresponds to that with the lowest energy gap for the well-known dissociation reaction into ionic lithium.[11,12] The energy gap for this particular reaction has also been determined experimentally by looking at the opposite association reaction.[13] Furthermore, the short-range PES for the ground state of LiH^+_2 has been computed and analytically fitted using different types of polynomial expansions[14] and has confirmed the general prediction that the complex has a stable geometry of C_{2v} symmetry and can be represented as a relatively weak complex between a H_2 molecule and the Li^+ ion. It therefore followed from that analysis that the association energy of LiH^+_2 with respect to the $Li^+ + H_2$ fragments was only 5.7 ± 8 kcal·mol^{-1}.[12]

In this work we deal with the above system using as a reference partner the neutral LiH. This approach leads us to the analysis of the global system in terms of its ground and first excited states using the full spatial extension of a Jacobi

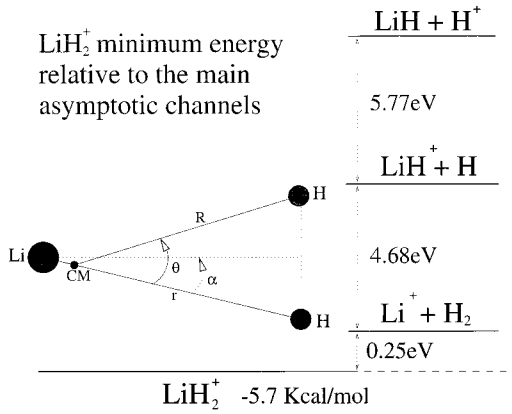

Figure 1. Geometry of the computational coordinates and relative energetics of the main asymptotic channels of LiH_2^+. See text for further details.

coordinate set centered on the "neutral" LiH molecule. In fact the ground state of the complex correlates with the $LiH^+ + H$ asymptotic state, while the first excited state goes, when the molecule and the proton are taken far apart, into the asymptotic channel with $LiH + H^+$ as fragments. Our knowledge of the relative ionization potentials for LiH (7.9 eV) and of H (13.67 eV) tell us that these channels should differ by about 5.7 eV. Hence the fragmentation[17] is about 10.7 eV above the LiH_2^+ stable structure. Figure 1 shows pictorially both the likely equilibrium structure of the triatomic complex and the relative energetics of three of the channels depicted in eqs 14 to 17.

It is interesting to note here that the computed minimum structure of the complex from ref 11 indicates the angles 2α to be 19.87°, the R_{H-H} distance to be 0.74 Å, and the distance from the lithium atom to the midpoint of the H−H diatomic, the R_{Li-H} distance, to be 2.14 Å. The CISD calculations of ref 14 produced similar values of 2α (21.2°) and of R_{Li-H_2} (2.04 Å). If one now converts these values into the Jacobian coordinates reported in Figure 1, i.e., the R distance and the θ angle, then one finds that the calculations of refs 11 and 14 yield the following values: $R \approx 1.85$ Å, $\theta \approx 27°$ and $r = 2.04$ Å. The present calculation, although not specifically looking for the absolute minima of the surface, suggest an overall minimum structure of LiH^+_2 with the following geometry: $R \approx 1.85$ Å, $\theta \approx 29°$ when we freeze r at 2.14 Å. Thus, without any explicit full optimization of the structure for the triatomic complex, we see that the present SCVB calculations come very close to yielding the minimum structure provided by the direct optimization approach. The corresponding stabilization energy with respect to the channel in eq 16 was computed to be about 4.87 eV, a value that compares well with the minimum energy of the lower surface which we have found in our calculations: 4.84 eV.

The present study intends to deal first with the energetics of the electronic potential energy surfaces associated with the LiH^+_2 system and the onset of its route to fragmentation into LiH and H^+. However an interesting feature of it is that with the data we collect here, one can also look at what happens when the system fragments into the ground-state asymptote $LiH^+ + H$. Our calculations provide us with a geometry of LiH that is very near to that of the equilibrium geometry of LiH^+. Hence this study also yields a description of the rigid rotor surface for the $LiH^+ + H$ colliding system. The chief reason for this choice is the interest in detecting possible sources of rovibrationally excited LiH or LiH^+ species that are expected to be emitted from the interstellar medium.[15,16] The lowest fragmentation channels, from eqs 14 and 15, on the other hand, would correspond instead to the formation of H_2 and H^+_2. These channels are of great interest in their own right and will be the subject of a separate study that we will be presenting elsewhere.[17]

3.2. The VB Calculation. We generated the surface on a dense numerical grid whose range in Jacobi coordinates is as follows: the distance between the center of mass of the molecule and the impinging projectile, R, varies between 1.75 a_0 to 15.0 a_0 for a total of 21 points on an slightly irregular grid; r, the internuclear separation in the LiH molecule varies from 2.3 a_0 to 4.3 a_0 in five points chosen to be inside the range determined by the two turning points of the $v = 4$ vibrational level of LiH; while θ, which is the angle between R and r, covers from 11° to 169° in twelve points corresponding to the abscissas of the Gauss−Legendre quadrature.

As we said before, we intend to focus first on the two states correlating with the asymptotic fragments $LiH + H^+$ and $LiH^+ + H$ corresponding to the excited and the ground states, respectively. Although the excited state will be the subject of our study in terms of its three Jacobi coordinates on the mentioned grid, as noted before, we also get some information on the behavior of the lower root that leads to the fragmentation into $LiH^+ + H$.

The basis set employed in the calculation consists of Li[10s4p2d/5s3p2d] and H[7s2p1d/5s2p1d] contracted Gaussian functions and it has already been adopted in our previous studies involving the LiH species.[18,19] For the $[LiH_2]^+$ complex the spin coupled wave function of the ground-state turns out to be

$$|\phi_{SC}\rangle = A\,[|\phi_{1s}\rangle|\phi'_{1s}\rangle|\phi_{H_A}\rangle|\phi_{H_B}\rangle|SM\rangle] \qquad (18)$$

where $|\phi_{1s}\rangle|\phi'_{1s}\rangle$ is a pair of orbitals localized on Li representing the $1s^2$ core of the atom and $|\phi_{H_A}\rangle|\phi_{H_B}\rangle$ is a pair of atomic orbitals localized on each of the hydrogen atoms. For the latter, the higher orbital energy corresponds to the more distant H atom, so that the SC orbital with the highest energy corresponds to the projectile when $R \gtrsim r$, while it belongs to the target hydrogen when $R \lesssim r$.

The ground state of the system therefore correctly describes the physical configuration $LiH^+ + H$ (with the positive charge localized on the Li atom) for all values of R. It then follows that when R and θ are small, the spin recoupling between the two H atoms can give rise to the reaction in eq 14 with H_2 production processes occurring via the formation of a short-range triatomic complex:

$$LiH^+ + H \rightarrow [LiH_2]^+ \rightarrow Li^+ + H_2 \qquad (19)$$

To obtain the reference SC wave function for the first excited state we have optimized a wave function in which four orbitals were maintained orthogonal to one orbital of the ground state. It turns out that, in all the geometries considered, the best *active* ground-state orbital is that with the highest orbital energy. The SC wave function of this state assumes the form

$$|\phi_{SC}\rangle = A[|\phi_{1s}\rangle|\phi'_{1s}\rangle|\phi_{H}\rangle|\phi_{Li}\rangle|SM\rangle] \qquad (20)$$

where $|\phi_{1s}\rangle|\phi'_{1s}\rangle$ is a pair of core orbitals of the Li atom coinciding with the ground state, $|\phi_H\rangle$ is the 1s orbital for the hydrogen closer to Li and $|\phi_{Li}\rangle$ is essentially the 2s orbital of lithium. Except for $R < r$ this wave function describes exactly the physical situation of a naked proton colliding with the LiH molecule.

For each reference function a set of *optimal virtual orbitals* was determined by the perturbative multiconfigurational ap-

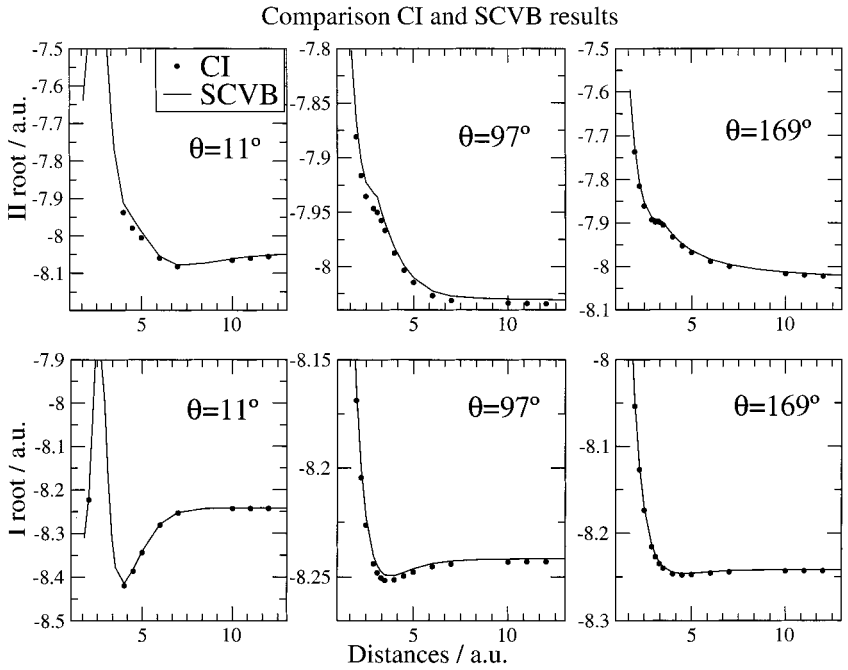

Figure 2. Comparison between the present SCVB calculations (solid lines) and of CI calculations (filled circles) as a function of R and for different values of orientation angles. The internuclear distance r was that of LiH at its equilibrium geometry.

proach cited above. The SCVB wave function was therefore constructed as a configuration interaction between the two reference functions of before and all the singly and doubly excited configurations of appropriate symmetry obtained from the reference configurations by vertical promotion to the optimal virtual orbitals previously calculated. To correctly describe the proton exchange region (i.e., when $R \approx r$), four additional configurations, obtained by single replacement of the valence orbitals of the SC excited state with that of the ground state, are added. In this way the final SCVB wave function is able to describe both of the configurations $LiH_A + H^+_B$ and $LiH_B + H^+_A$ representing the interacting state at small R values. By adding a set of ionic configurations, the final SCVB wave function is constructed via 84 configurations, corresponding to a total number of 125 VB structures.

The SCVB curves for the ground state and for the excited states are reported in Figure 2 where the full CI calculations corresponding to the same basis set are also included. It is evident from this figure that there is very good agreement between the two sets of calculations: in particular the irregularity at short range shown by the full CI surfaces also appears in the corresponding SCVB curve, where it can be assigned to the change of the active space (from 1s centered on the projectile to the 1s orbital centered on the H of the target). The active space change leads to the description, via eq 20, of $LiH^+ + H$ with the positive charge localized on the H atom of the target LiH so that it is possible to state that the irregularity is merely a representation of the activation barrier for the charge-transfer reaction:

$$LiH_A + H^+_B \rightarrow LiH_B + H^+_A$$

A perusal through the results of Figure 2 for the ground and the excited states shows that the SCVB and the full-CI PES proceed substantially parallel as a function of R and θ, although we know that the full CI calculations require a higher computational cost since the number of determinants in the present instance, 1 654 650, is indeed considerable, even when the smallness of the basis set employed is taken into account. On the whole, we found the differences between the SCVB and the full CI values to be almost invariably between 0.002 and 0.004 hartrees for the ground state and for the excited state respectively, so that the transition energies differ by about 0.05 eV. It is evident that the SCVB wave function maintains a reasonable computational cost while ensuring an acceptable accuracy with respect to the more expensive full-CI method, a fact that makes it suitable for the analysis of the dynamic properties of the $LiH(LiH^+) + H^+(H)$ system as we shall further discuss below.

4. The Rovibrational Potential

As we have mentioned earlier, the study of the spatial features of the LiH^+_2 system implies a review of the energetics of several asymptotic channels, as outlined in eqs 14, 16, and 17 and depicted in Figure 1 within the short-range and intermediate-range regions of their interaction. If we consider the possibility of producing detectable rovibrationally excited LiH/LiH^+ molecules[15,16] as a consequence of a collision or a half-collision involving the formation of the triatomic complex in either its ground or excited state, then the dynamic processes are affected by the couplings existing between the Jacobi coordinates. The present calculations can provide us with useful information about the collisional efficiency in producing excitation of the two molecular asymptotic fragments by first showing us the strength of the overall interaction as a function of the R,r,θ coordinates reported in Figure 1.

4.1. The Orientational Anisotropy. If we consider the overall behavior of two of the Jacobi coordinates when keeping the internuclear distance of LiH at a fixed value, then we recover the orientational behavior for the rigid-rotor potential (RR) energy surface that corresponds to the electronically induced coupling between the R and the θ coordinates.[20] From previous study on the diatomic fragments,[21] we know that the r_{eq} value for the ground electronic state of LiH is of 3.014 a_0 while the value for the LiH^+ is 4.101 a_0.

The upper surface produced by the present calculations at $r = r_{eq}(LiH)$ describes the RR surface for the system composed by the asymptotic fragments LiH and H^+. An overall view of such orientational anisotropy is shown in Figure 3 for both

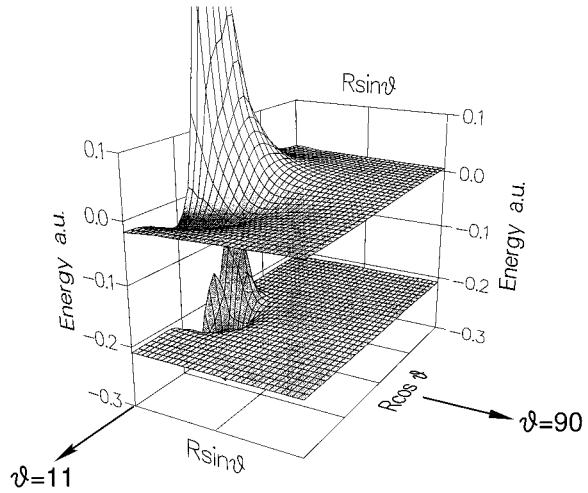

Figure 3. Three-dimensional view of the two surfaces as a function of cylindrical coordinates where $x = R \sin\theta$ and $y = R \cos\theta$. The internuclear distance r was that of LiH at its equilibrium geometry.

surfaces, separated by the 5.7 eV energy gap already reported in Figure 1. We clearly see there that the corresponding lower PES describes the electronic ground state of the ionic complex with the marked minimum corresponding to $\theta = 29°$, while the upper surface corresponds to the excited state of the system correlating asymptotically with $LiH + H^+$. The large energy gap precludes any crossing with the ground state and therefore we conclude that a possible transfer into the lower electronic state could only proceed radiatively with the final formation of $LiH^+ + H$ or $H_2 + Li^+$.

If one now carries out an analysis for the upper surface when the r coordinate is fixed at the diatomic geometry of the neutral LiH ($r = 3.014\ a_0$) i.e., for the orientations that characterize the $LiH + H^+$ asymptotic channel, one can extract useful information on the rotational anisotropy that should also remain reasonably valid for other r values. An example of the computed behavior is shown in Figure 4, where we report the strength of the coupling potential as a function of the main radial coordinate and for different values of the orientational angle. It is interesting to note here that, since we are dealing with an electronically excited state, the interaction energies are less stabilizing than those shown by the electronic ground state where the more compact structure of the neutral LiH in close quarters causes a dominance of the repulsive interaction. Thus, although we see that the most stable structures occur in the small angle region of the upper left panel, beyond $\theta \approx \pi/2$ the interaction becomes essentially repulsive as it is driven by the dominant dipole−charge interaction which acts in the long-range region and which is related to the contribution of the electrostatic multipole proportional to $P_1(\cos\theta)R^{-2}$. It therefore follows that the corresponding anisotropy is rather marked and extends over the whole angular region examined by the calculations.

A comparative analysis of the angular anisotropy of the two PESs is presented in Figure 5, but this time over a larger radial range and listing instead the total energy values for the two PESs. In both surfaces the intermolecular distance is kept fixed at the equilibrium value of the neutral species. One clearly sees that for both electronic states the energy changes are most marked in the small angle region as the orientation of the impinging projectile (H^+ or H) varies. On the other hand, as the angles move to the larger values with θ up to 82°, one sees that the lower surface (corresponding to the ground state) shows a much less evident anisotropy as the hydrogen atom leaves the LiH^+ partner.

We had already seen that the lower surface of Figure 3 dissociates into the $LiH^+ + H$ fragments, thus making it reasonable to analyze its orientational anisotropy for diatomic geometries close to those of the LiH^+ partner. We thus present in Figure 6 a similar analysis for the surface where the r value is fixed at 4.3 a_0. One clearly sees in the top two panels how markedly the shape and strength of the short-range and intermediate-range interactions change with the value of θ, since small angular values correspond to the stable triangular structure with the two hydrogen atoms close to each other. As already noted for the other geometry, beyond the $\theta \approx \pi/2$ values one detects (see the lower two panels) a much weaker dependence of the interaction on the orientation: the potential curves, in fact, appear to be essentially unchanged in the angular quadrant that ends on the lithium side approach.

A more global behavior of the two surfaces can be seen from the comparison between the two roots of the VB calculations shown in Figure 7, where we can see the RR behavior of the $LiH^+ + H$ asymptote (lower curve) and the stretched diatom state for the $LiH + H^+$ (upper curve): we report in it the same angular range of Figure 5. The lower root clearly shows that its angular dependence is more marked in the small-angle region, while the upper root appears to have a stronger anisotropy that extends well beyond that region and exists over a greater range of radial distances. A simple, qualitative explanation for these differences of behavior could be provided by examining the leading terms of the long-range interactions for the two fragmentation channels. In the case of the lower root, the induced forces contain the interaction between the spherical polarizability of the H atom and the charge of the LiH^+, with spherical symmetry and an R^{-4} behavior. On the other hand, in the upper curve we have the previously mentioned term due to the charge−dipole interaction with its longer-range contribution (R^{-2}), and a fairly large coefficient ($\mu_{LiH} = -2.32$ a.u.) that directly influences directly the anisotropy of the interaction potential in the long-range region, via its dependence on the $P_1(\cos\theta)$ polynomial.

The differences in the strength of the orientational anisotropy for the two PES's over the radial range of action of the potential could be seen also from Figure 8. In this figure we report the total energy of the system as a function of the orientation angle θ, for different values of the R distance and for r equal to the LiH equilibrium internuclear distance. In its upper left panel, corresponding to the small R region, one sees that both systems present a strong coupling between the molecular partners and the approaching atomic components, with the upper surface showing however a stronger coupling due to the orientational anisotropy.

In fact, if one defines the local angular torque, $F_\theta(R)$ as given by

$$F_\theta(R) = -\frac{\partial V(R,\theta)}{\partial \theta}\Big|_{R=R_1} \qquad (21)$$

at chosen R_1 values, then one sees that this quantity is larger for the second root in comparison with the first root and that it extends over a broader range of angles. The angular torque (in arbitrary units) is plotted in Figure 9 for different values of R_1, as a function of θ with fixed internuclear distance of LiH at the equilibrium value for both surfaces. The lower panel refers to the short-range region where one clearly sees that the torque is usually larger for the lower of the two surfaces and stronger in the latter when the proton is approaching the H side of the molecule (small angle region). The upper panel shows the behavior of the same quantity in the long-range region where,

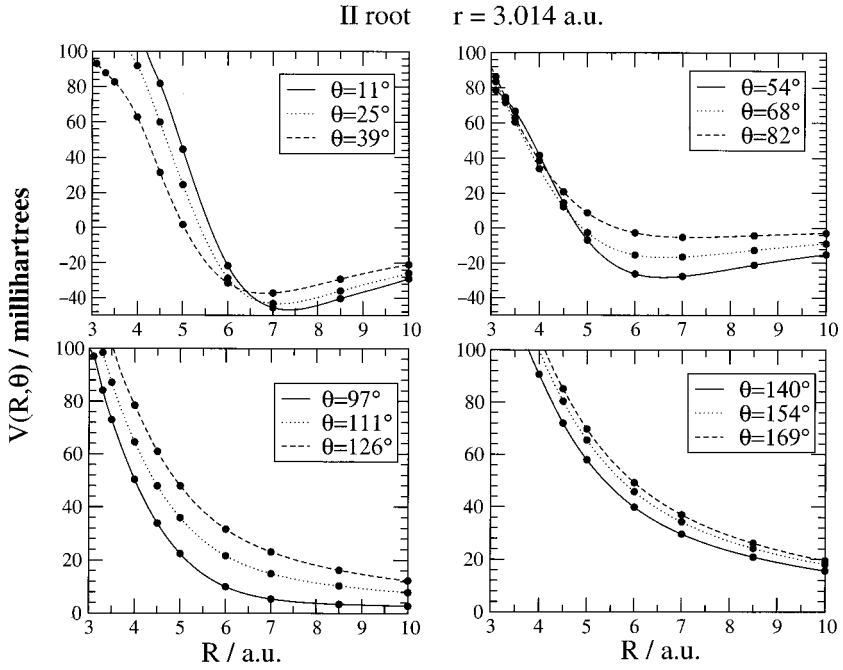

Figure 4. Computed orientational behavior of the upper PES as a function of the two coordinate θ and R . The internuclear distance r was that of LiH at its equilibrium geometry hence kept fixed at 3.014a.u.

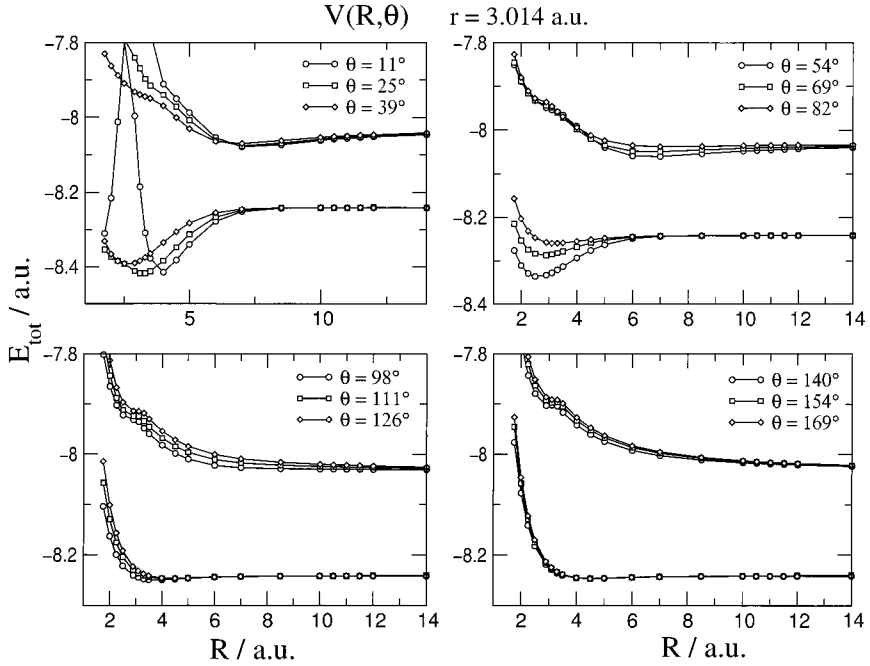

Figure 5. The same as in Figure 4 but now in terms of total energies and showing the two roots to allow a direct comparison.

on the contrary, the second root shows a stronger torque over the whole range of θ. In conclusion, an analysis of the orientational anisotropy of the two surfaces indicates that both of them exhibit strong anisotropic features, with the excited state being the one with the greater radial range of that anisotropy but with the a less marked angular variation of the torque.

We also see that, at least in the region of relative geometries sampled by the (R , θ, $r = r_{eq}$) grid considered here, no evidence exists for any avoided crossing between the two roots, although the possibility exists that it may appear when a broader range of r values is considered. As we shall see below, however, this is not the case and therefore the radiation-induced transition between the two states remains so far the more likely possibility, especially given the considerable dipole moments of both diatomic fragments.

4.2. The Vibrational Coupling. As we mentioned before, the full PES discussed in this work also includes the explicit dependence of the interaction on the internuclear distances of the LiH molecule. It is the effect of the change of r that explicitly gives us the vibrational coupling produced within each surface. A pictorial example of this quantity is given by the results reported in the four panels of Figure 10 where we note the following:

(1) If one considers the small angle region of the left panels one immediately sees that, in the lower surface, as the distance between the H and the molecule increase, the dependence of the potential on the molecular stretching motion becomes weaker. This indicates, as often noted,[20] the chiefly short-range nature of the vibrational-to-translational (V−T) coupling terms;

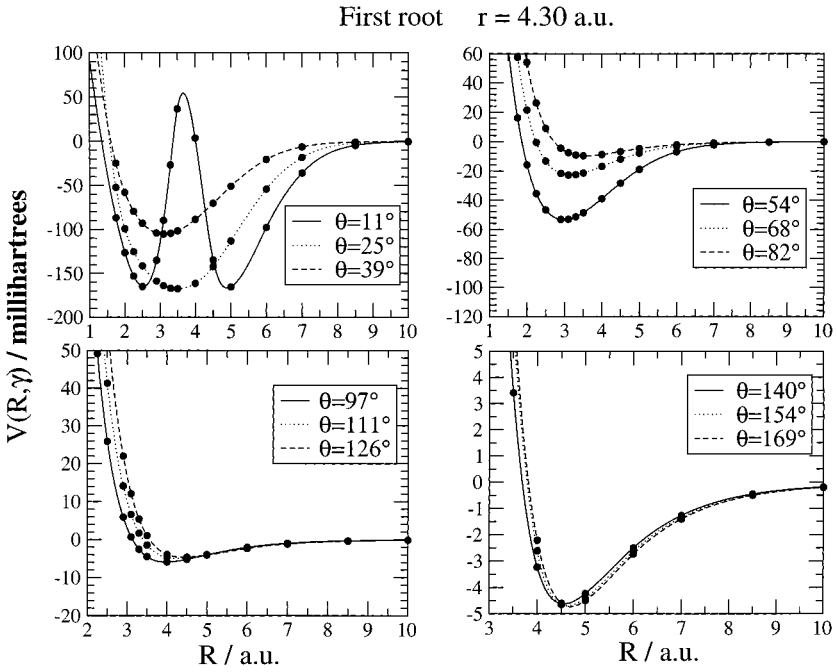

Figure 6. Same calculations as in Figure 4 but for the lower surface and for $r = 4.30$ a.u.

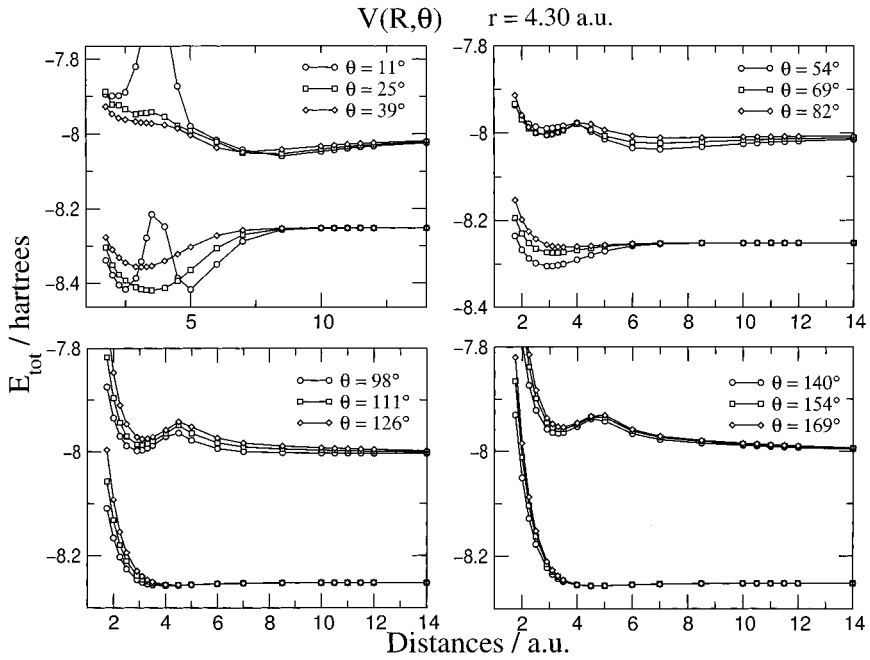

Figure 7. Same computed comparison as that shown in Figure 5. Here the LiH internuclear distance, *r*, is kept at 4.30 a.u.

(2) The upper PES shows that the coupling remains stronger as the angle varies (see left panel) and that it is also nonnegligible at the larger distances (displayed in the lower panels). The charge−dipole interaction obviously plays a dominant role in creating a more marked V−T coupling;

(3) The lower PES shown at the larger angle in the right panels indicates that the vibrational coupling depends little on the relative distance and is also fairly weak beyond the shorter distances displayed in the two left panels. The features shown suggest that the lower PES corresponds to weaker V−T coupling at the larger distances and away from a small angular cone on the Li-side of the molecule;

(4) In the lower right panel, we have also shown the $v = 0$ and $v = 5$ vibrational wave functions of the isolated LiH molecule. For distances of the order of 8.0 a_0, and for the $\theta = 169°$, we see that we can almost neglect the coupling coming from the residual interaction between the LiH molecule and the proton. The monotonic long-range electrostatic interaction simply causes our calculated potential to be an intermolecular LiH potential shifted by the charge−dipole contribution. This is not true for the $\theta = 11°$ orientation for which, as one can see in the lower right panel, a *chemical* interaction still exists from the strong coupling between the two fragments and it gives rise to the potential well shown by the upper surface. The lower surface, on the other hand, represents a compressed LiH^+ bond, that then causes the potential to be almost flat in the minimum region. What the calculations, therefore, indicate is the existence of rather marked couplings between *R* and *r* over the range of the examined coordinates and thus the presence of an overall interaction that should produce dynamic outcomes with sizable flux going into rovibrationally excited molecular states.

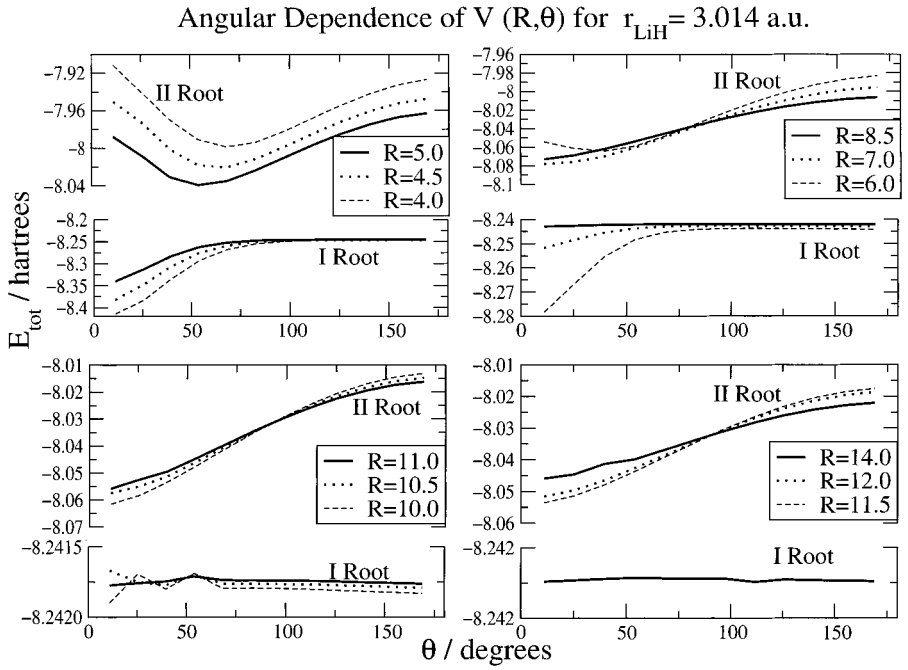

Figure 8. Comparison of the angular dependence of the two PES's computed in this work for different values of the *R* coordinate. The LiH distance was kept fixed as that of the neutral molecule at its equilibrium geometry.

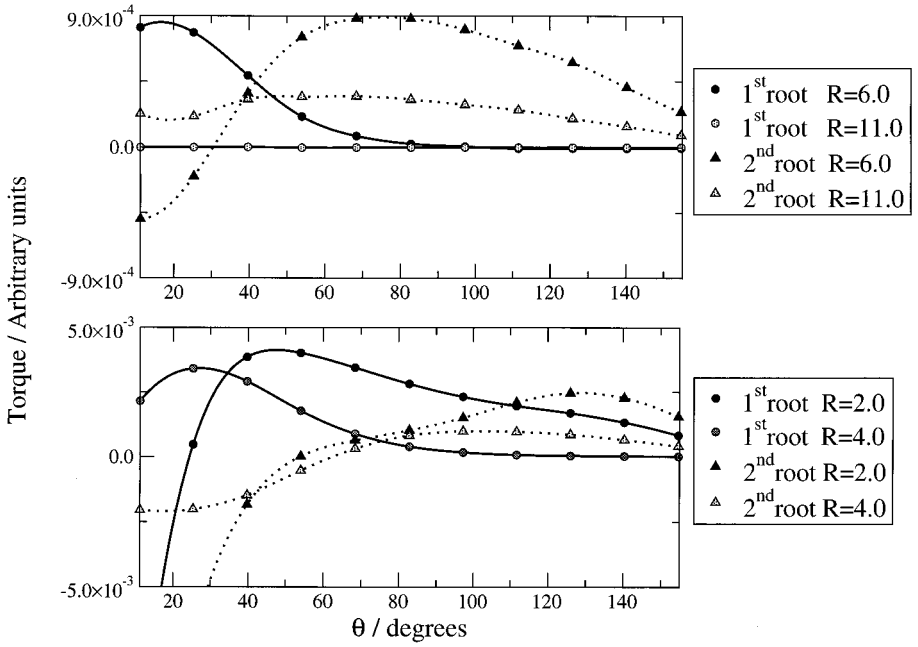

Figure 9. The torque acting on the molecule for different values of the *R* coordinate as a function of the orientation angle θ. We have chosen two values of *R* in the short-range (lower panel) and two in the long-range regions (upper panel). The lines connecting points at which we calculated the first derivative of the potential are solid lines for the first root and dotted lines for the second one.

5. Charge-Transfer Features

We have mentioned several times in the previous discussion that the difference between the LiH and H ionization potentials (respectively 7.9 eV and 13.6 eV) causes the asymptotic energy gap between the two electronic states and keeps them well separated, within the coordinate space of interest in the present study. As a consequence of these features, we therefore expect the behavior of the electronic densities in the two adiabatic roots to be different in the range of coordinates spanned by the present calculation.

A pictorial view of such differences is given in Figure 11, where we report the variation of the Mulliken charge populations[22] on the three atomic centers as a function of orientation and of the relative atom−molecule distance *R*. The internuclear coordinate has been kept fixed at the equilibrium value of LiH in order to simplify the presentation. We only report in Figure 11 two of the orientations we have examined since the behavior of the Mulliken populations changes rather smoothly across the angular range.

When looking at the ground electronic state (two lower panels) one sees that the system is qualitatively well described, in both orientations, by the conventional formula H−Li^+···H, where the possible charge is located on the lithium atom over the whole range of relative distances. Therefore the small angle region closer to the expected C_{2v} geometry of the ground state of the $[LiH_2]^+$ complex shows an arrangement of charges that

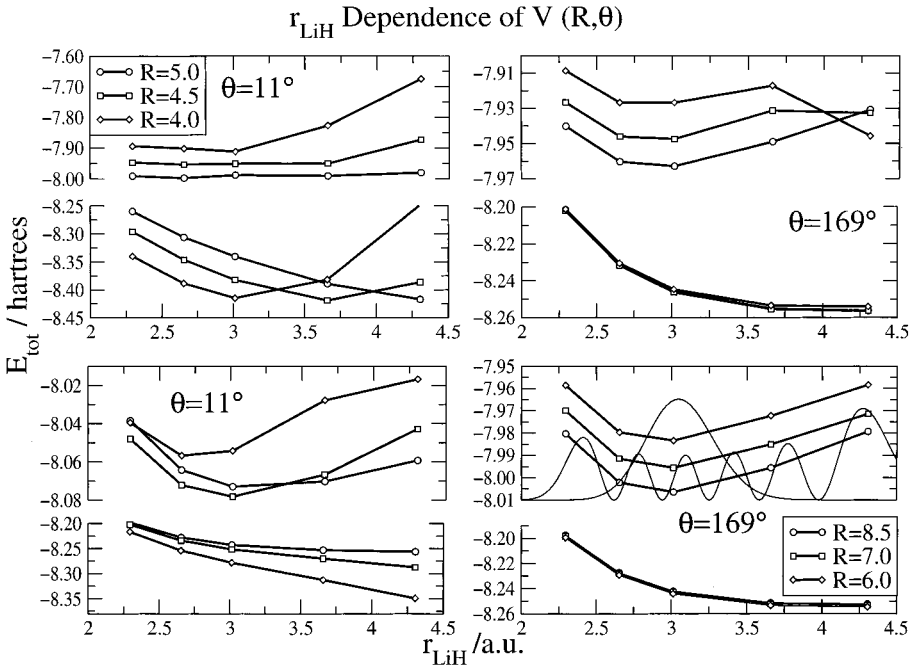

Figure 10. Computed vibrational dependence of the two PES's as a function of relative distances R and for two different relative orientations: $\theta = 11°$ (left panels) and $\theta = 169°$ (right panels).

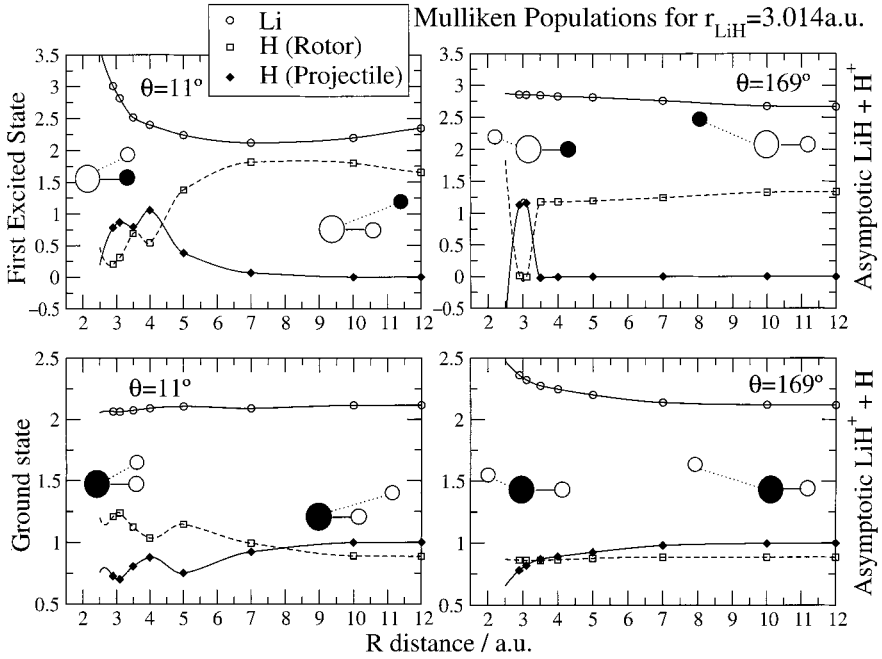

Figure 11. Computed Mulliken populations for the LiH partner, at a fixed geometry, as a function of R and for two orientations ($\theta = 11°$, 169°). The two lower panels refer to the first root while the upper ones to the second root. The r value was chosen to be that of LiH at its equilibrium geometry. The black circles in the triatomic schemes indicate the atoms on which most of the positive charge is localized.

corresponds to a sort of $Li^+\cdots H_2$ situation. As R increases, however, we see that the two H atoms carry different charges and tend to foreshadow the charge configuration of the breakup channel given by $LiH^+ + H$. The large angle approach shows clearly, in the lower right panel, a more regular behavior of the electronic populations, since now the H atom approaches by the Li side and provides, in the range of the smaller R values, the presence of a charged hydrogen being added to a weakly charged Li before the Li^+ formation in the $LiH^+ + H$ final dissociation.

The behavior of the excited state is quite different and is shown in the upper panels of Figure 11; one sees there more clearly the effects of electronic distortion during the approach of the proton. In the small angle region the system undergoes a marked and rapid charge variation as one H atom is added to the complex: thus while in the asymptotic region the arrangement corresponds to that of a naked proton and a neutral LiH molecule, during the collision the positive charge is transferred to the H atom previously belonging to the LiH molecule. In the large-angle region the charge exchange between the two H atoms is more clear and takes place in a small range of R values, while this time the lithium atom remains nearly neutral. In this latter case one can think of a flow of electronic charge between the two H atoms via a sort of through-bond charge migration. Between 2.5 and 3.5 a.u., in fact, the two hydrogen atoms exchange one unit of charge and fairly rapidly reach a situation

where H^+ is removed from a neutral LiH system. This situation is, probably, the direct consequence of a strong nonadiabatic interaction with a third electronic state that crosses the second root. It is very likely that this third root correlates with an excited state of LiH and a H^+ atom in the asymptotic region when r remains within values similar to those employed by our calculation. This electronic state, as R is decreased, becomes essentially an excited state of LiH^+ with the positive charge localized on the hydrogen side and in the presence of an additional H atom. The nonadiabatic coupling between these two excited surfaces is responsible for the bumps appearing at the larger angular values and at the larger r values in the second root (e.g. see Figures 5 and 7).

The above analysis shows that the chemical reaction leading to a charge transfer process between the ground state of LiH^+ and LiH is prevented by the large energy gap separating the two surfaces at least for intramolecular distances close to the near-equilibrium geometry of the LiH/LiH^+ partners. This charge transfer however could become effective if one considers different r geometries as, for example, those spanned by very large r values that correspond to LiH being highly vibrationally excited or to fairly stretched LiH^+ bond distances. In conclusion, this qualitative analysis, although still preliminary, can lead us to say that the charge transfer process is not likely to be effective during the breakup of LiH_2^+, and one could expect low values for the rate constant of the charge-transfer reaction shown in eq 3.

With the same token we can also say that the reaction eq 4 listed earlier, or, more precisely the process

$$LiH + H^+ \rightarrow H_2 + Li^+$$

is not likely to take place without the occurrence of a radiative transition to the ground electronic surface, while the only possible reactive outcome for $LiH + H^+$ seems to be $H^+_2 +$ Li. The peculiar electronic structure of the system forces us to reconsider the possible chemical processes that are deemed to be important for lithium chemistry in the medium which is supposed to have existed in the early universe.[6]

6. General Conclusions

We have analyzed in some detail the behavior of two of the electronic states of the $[LiH_2]^+$ complex. The energetics of the system has been analyzed considering either a collision or a half-collision (fragmentation) situation for the molecules and the atomic partners that make up the possible asymptotic arrangements, $LiH + H^+$ and $LiH^+ + H$. We have excluded, for the moment, an analysis of the asymptotic channels $(Li + H_2)^+$ since our calculation is not sufficiently extensive to include the relevant reactive configuration space. The calculations employed an extended, nonorthogonal configuration interaction expansion within a spin-coupled valence bond approach. We have looked into the dependence of the interaction potential on the angular orientation, on the internuclear distance of the LiH/LiH^+ molecules, and on the relative distances between the two asymptotic partners. The results indicate, as expected, rather marked differences between the two surfaces that lead to the two different asymptotic arrangements. In particular:

(1) The lower root shows a short-range orientational anisotropy, with a dominance of the spherical polarization of the H by the LiH^+ charge at the larger distances. Likewise, the small angle region $\theta < \pi/2$ exhibits the stronger effects of the orientational changes on the potential energy;

(2) The upper electronic state, on the other hand, shows a more marked and more long-range orientational anisotropy. The charge−dipole interaction here plays an important role and dominates the features of the upper potential energy curves;

(3) The dependence of the interaction on the vibrational coordinate also turns out to be rather different for the two roots. Thus we found that the excited state affords stronger coupling between r and R than that shown by the ground state (where however we only considered the effect of bond compression).

The above analysis, together with the effects from internal charge migration during the approach of the projectiles to the targets, indicates that these interactions could reasonably produce rovibrationally hot LiH/LiH^+ molecules. A direct use of the upper surface over the range of coordinates necessary for a full quantum study of the excitation/relaxation dynamics of the neutral target is presently being carried out in our group and will be presented elsewhere.[23]

From the above analysis we can also say that the large energy gain during a near-collinear approach ($\theta \approx 0$) of an H atom to LiH^+ could reasonably lead to the formation of $Li^+ + H_2$, thus making the study of the subreactive collisional dynamics of $LiH^+ + H$ of rather limited interest unless one also were to consider the H_2 formation reaction.

Another point that is brought out by the charge migration/exchange analysis described in the present work involves the process of eq 3. The present calculations give no indication of curve-crossing features; hence one should expect that the way in which the charge transfer reaction might occur would be via a one-photon emission process, with consequent decay to the ground state. However, without specific computations, this route remains largely speculative.

Finally, all the numerical values of the computed PES's of the present work are available upon request to the corresponding author.

Acknowledgment. The financial support of the Italian National Research Council (CNR) and of the Italian Ministry for University and Research (MURST) is gratefully acknowledged. F. A. G. also thanks the Max Planck Society for the award of the Max Planck Research Prize that was also employed to partly finance the present research.

References and Notes

(1) Shu, F. M. *The Physics of Astrophysics*; University Books: Chicago, 1991; Vol. 1.

(2) Lepp, S.; Shull, J. M. *Astrophysics. J.* **1984**, *280*, 465.

(3) Dalgarno, A.; Kirby, K.; Stancil, P. C. *Astrophysics. J.* **1996**, *458*, 397.

(4) Gianturco, F. A.; Gori, G. P. *Astrophysics. J.* **1997**, *479*, 560.

(5) Stancil, P. C.; Lepp, S.; Dalgarno, A. *Astrophysics. J.* **1996**, *458*, 401.

(6) Galli, D.; Palla, F. *Astron. Astrophys.* **1998**, *335*, 403.

(7) Buonomo, E.; Kumar, S.; Gianturco, F. A.; Clarke, N. J.; Sironi, M.; Raimondi, M. *Chem. Phys.* **1998**, *231*, 350.

(8) Bodo, E.; Gianturco, F. A.; Martinazzo, R. in preparation.

(9) Cooper, D. L.; Gerrat, J.; Raimondi, M. *Adv. Chem. Phys.* **1987**, *69*, 319.

(10) Cooper, D. L.; Gerrat, J.; Raimondi, M. *Chem. Rev.* **1991**, *91*, 929.

(11) Hobza, P.; Von, R. Scheyer, P. *Chem. Phys. Lett.* **1984**, *105*, 6.

(12) Dixon, D. A.; Gole, J. L.; Komornicki, J. *Phys. Chem.* **1988**, *92*, 1378.

(13) Wu, C. H. *J. Chem. Phys.* **1979**, *71*, 783.

(14) Searles, D. J.; Von Naghy-Felsobuki, E. I. *Phys. Rev. A* **1991**, *43*, 3365.

(15) Maoli, R.; Ferrucci, V.; Melchiorri, F.; Signore, M.; Tosti, D. *Astrophys. J.* **1996**, *457*, 1.

(16) Maoli, R.; Melchiorri, F.; Tosti, D. *Astrophys. J.* **1994**, *458*, 372.
(17) Bodo, E.; Martinazzo, R. in preparation.
(18) For example, see: Gianturco, F. A.; Kumar, S.; Pathak, S. K.; Raimondi, M.; Sironi, M.; Gerrat, J.; Cooper, D. L. *Chem. Phys.* **1977**, *215*, 227.
(19) Bodo, E.; Kumar, S.; Famulari, S.; Raimondi, M.; Sironi, M. *J. Phys. Chem.* **1998**, *102*, 9390.
(20) For example, see: Gianturco, F. A. *The Transfer of Molecular Energy by Collision*; Spinger Verlag: Berlin, 1979.
(21) Gianturco, F. A.; Gori, G. P.; Berriche, H.; Gadea, F. X. *Astron. Astrophys.* **1996**, *117*, 377.
(22) McWeeny, R. *Methods of Molecular Quantum Mechanics*; Academic Press: London, 1989.
(23) Bodo, E.; Gianturco, F. A.; Martinazzo, R. in preparation.